Title

Rational rotation-minimizing frames—Recent advances and open problems

Journal

Applied Mathematics and Computation, 272(P1)

ISSN

0096-3003

Author

Farouki, Rida T

Publication Date

2016

DOI

10.1016/j.amc.2015.04.122

Peer reviewed

Rational rotation-minimizing frames — recent advances and open problems

Rida T. Farouki
Department of Mechanical and Aerospace Engineering,
University of California, Davis, CA 95616, USA.

Abstract

Recent developments in the basic theory, algorithms, and applications for curves with *rational rotation–minimizing frames* (RRMF curves) are reviewed, and placed in the context of the current state–of–the–art by highlighting the many significant open problems that remain. The simplest non–trivial RRMF curves are the quintics, characterized by a scalar condition on the angular velocity of the *Euler–Rodrigues frame* (ERF). Two different classes of RRMF quintics can be identified. The first class of curves may be characterized by quadratic constraints on the quaternion coefficients of the generating polynomials; by the root structure of those polynomials; or by a certain polynomial divisibility condition. The second class has a strictly algebraic characterization, less well–suited to geometrical construction algorithms. The degree 7 RRMF curves offer more shape freedoms than the quintics, but only one of the four possible classes of these curves has been satisfactorily described. Generalizations of the *adapted* rotation–minimizing frames, for which the angular velocity has no component along the tangent, to *directed* and *osculating* frames (with analogous properties relative to the polar and binormal vectors) are also discussed. Finally, a selection of applications for rotation–minimizing frames are briefly reviewed — including construction of swept surfaces, rigid–body motion planning, 5–axis CNC machining, and camera orientation control.

Keywords: rotation–minimizing frame; Pythagorean–hodograph curve; angular velocity; quaternions; Hopf map; spatial motion design.

e–mail: farouki@ucdavis.edu

1 Introduction

The characterization of the spatial motion of a rigid body involves specifying its *position* and *orientation* as functions of time. The path of a distinguished point (e.g., the center of mass) may be used to specify the variation of position as a parametric curve $\mathbf{r}(t)$. To describe the variation of orientation, one may employ an orthonormal frame $(\mathbf{f}_1(t), \mathbf{f}_2(t), \mathbf{f}_3(t))$ embedded in the body. When the parameter t represents *time*, the first and second curve derivatives define the velocity and acceleration of the body, and the frame derivatives define its angular velocity and acceleration. For a general parameterization, the chain rule must be used to determine physical velocities and accelerations.

The most general rigid–body motion admits independent specification of position and orientation. In a variety of contexts, however, it is desirable or natural to consider motions that involve a correlation between them. Among such constrained spatial motions, those based on *rotation–minimizing frames* are of special interest. In general terms, they are characterized by specifying a unit vector field $\mathbf{v}(t)$ along the path $\mathbf{r}(t)$, and requiring the angular velocity $\boldsymbol{\omega}(t)$ of the frame $(\mathbf{f}_1(t), \mathbf{f}_2(t), \mathbf{f}_3(t))$ to maintain a vanishing component along the prescribed direction $\mathbf{v}(t)$ — i.e., the constraint $\mathbf{v}(t) \cdot \boldsymbol{\omega}(t) \equiv 0$ is satisfied. Intuitively, this means that the frame vectors have no instantaneous rotation about $\mathbf{v}(t)$ upon traversing the curve $\mathbf{r}(t)$. In many cases of practical interest, the direction field $\mathbf{v}(t)$ coincides with one of the frame vectors.

A familiar frame on a space curve is the *Frenet frame* $(\mathbf{t}, \mathbf{p}, \mathbf{b})$ comprising the tangent $\mathbf{t}$ defining the instantaneous direction of motion along the curve, the principal normal $\mathbf{p}$ pointing to the center of curvature, and the binormal $\mathbf{b} = \mathbf{t} \times \mathbf{p}$ [44]. This frame is rotation–minimizing with respect to $\mathbf{p}$ — i.e., $\mathbf{t}$ and $\mathbf{b}$ exhibit no instantaneous rotation about $\mathbf{p}$ as we traverse the curve. When the normal–plane vectors $\mathbf{p}, \mathbf{b}$ are replaced by vectors $\mathbf{u}, \mathbf{v}$ in that plane having no instantaneous rotation about $\mathbf{t}$, we obtain a rotation–minimizing *adapted* frame $(\mathbf{t}, \mathbf{u}, \mathbf{v})$ — also known as a *Bishop frame* [3]. A frame $(\mathbf{f}, \mathbf{g}, \mathbf{b})$ retaining the binormal $\mathbf{b}$ but replacing the vectors $\mathbf{t}, \mathbf{p}$ in the osculating plane (i.e., the plane that most nearly contains the curve at each point) by vectors $\mathbf{f}, \mathbf{g}$ in that plane having no instantaneous about $\mathbf{b}$, is a rotation–minimizing *osculating* frame [20]. Other types of rotation–minimizing frame, not based on modifying the Frenet frame, are also possible. For example, the rotation–minimizing *directed* frame comprises the *polar vector* $\mathbf{o}(t) = \mathbf{r}(t)/|\mathbf{r}(t)|$ and two vectors $\mathbf{p}(t)$, $\mathbf{q}(t)$ spanning the *image plane* orthogonal to $\mathbf{o}(t)$, that have no instantaneous about it. Such frames are of interest in defining the motion

of a camera that images a stationary object located at the origin [15].

Among these different frames, the rotation–minimizing adapted frame has by far received the most attention, motivated by its applications in robotics, computer animation, swept surface constructions, spatial motion planning, and related fields. Many methods for the approximation of such frames have been proposed [23, 34, 35, 36, 37, 40, 43, 50, 52, 53, 55]. However, recent years have witnessed a growing interest in the characterization and construction of *exact* (i.e., rational) rotation–minimizing frames on space curves. The goal of this study is to survey recent results in this area, and to assess the prospects for further advances in basic theory, algorithms, and applications. Obviously, it is impractical to include complete details of proofs and derivations here, for which the reader may consult the cited references. Instead, the focus is on a succinct but comprehensive enumeration of the new results, identifying their inter–relationships, and highlighting the open problems they pose.

The plan for the remainder of this paper is as follows. Following a synopsis of the rotation–minimizing frame (RMF) problem in Section 2, a brief review of the properties of spatial Pythagorean–hodograph (PH) curves is presented in Section 3. The PH curves play a fundamental role in the identification of space curves with rational adapted RMFs, since only PH curves have rational unit tangents. In particular, PH curves admit a rational adapted — but not rotation–minimizing — frame, the *Euler–Rodrigues frame* (ERF), that serves as a reference for identifying rational adapted RMFs. The angular velocity of the ERF is reviewed in Section 4, and used to express an existence condition for PH curves with rational rotation–minimizing adapted frames — or *RRMF curves*. Based on this result, Section 5 gives an account of the current state of knowledge concerning low–degree RRMF curves. Other RMF types, namely the *osculating* and *directed* frames, are briefly reviewed in Section 6. Finally, Section 7 describes some applications of the RRMF curves, while Section 8 enumerates desiderata in the existing theory and algorithms.

2 Many ways to frame a space curve

The first systematic study of space curves — regarded[1] as "curves of double curvature" — is found [4] in the *Recherches sur la courbes à double courbure* of Alexis Claude Clairault (1713–1765), as presented to the French Académie des Sciences at the age of sixteen. Essentially, a space curve C is determined

[1]This term was first introduced by Henri Pitot (1695–1771) in 1724.

by defining x and y as functions of z, the "double curvature" referring to the individual curvatures of the planar curves defined by these functions, i.e., the projections of C onto the (x, z) and (y, z) planes. A key point recognized in Clairault's work is that, while a smooth space curve has a unique tangent at each point, there are infinitely many normals, defining the *normal plane*.

Further elucidation of the geometry of space curves was contingent on the development of calculus, culminating in the theory of *differential geometry*. In particular, a consideration of the first three derivatives of the arc–length parameterization $\mathbf{r}(s) = (x(s), y(s), z(s))$ of a space curve, satisfying

$$\left(\frac{\mathrm{d}x}{\mathrm{d}s}\right)^2 + \left(\frac{\mathrm{d}y}{\mathrm{d}s}\right)^2 + \left(\frac{\mathrm{d}z}{\mathrm{d}s}\right)^2 \equiv 1\,,$$

leads to the identification of three mutually orthogonal intrinsic directions at each point of a space curve — the tangent, principal normal, and binormal. The variation of the orthonormal frame specified by these directions can be completely characterized by two scalar functions, the *curvature* $\kappa(s)$ and the *torsion* $\tau(s)$, which uniquely determine a space curve with a prescribed initial point and tangent. These developments were first elucidated [39] in the work of Michel–Ange Lancret (1774–1807), Augustin–Louis Cauchy (1789–1857), Fréderic–Jean Frenet (1816–1900), and Joseph Alfred Serret (1819–1885).

In modern terms, the *Frenet–Serret frame* $(\mathbf{t}, \mathbf{p}, \mathbf{b})$ comprising the tangent $\mathbf{t}$, principal normal $\mathbf{p}$, and binormal $\mathbf{b}$ is specified [44] in terms of a general parameterization $\mathbf{r}(\xi) = (x(\xi), y(\xi), z(\xi))$ by

$$\mathbf{t} \,=\, \frac{\mathbf{r}'}{|\mathbf{r}'|}\,, \quad \mathbf{p} \,=\, \frac{\mathbf{r}' \times \mathbf{r}''}{|\mathbf{r}' \times \mathbf{r}''|} \times \mathbf{t}\,, \quad \mathbf{b} \,=\, \frac{\mathbf{r}' \times \mathbf{r}''}{|\mathbf{r}' \times \mathbf{r}''|}\,, \tag{1}$$

and its variation along the curve is characterized by the relations

$$\frac{\mathrm{d}\mathbf{t}}{\mathrm{d}\xi} \,=\, \sigma\kappa\,\mathbf{p}\,, \qquad \frac{\mathrm{d}\mathbf{p}}{\mathrm{d}\xi} \,=\, \sigma(\tau\,\mathbf{b} - \kappa\,\mathbf{t})\,, \qquad \frac{\mathrm{d}\mathbf{b}}{\mathrm{d}\xi} \,=\, -\,\sigma\tau\,\mathbf{p}\,, \tag{2}$$

the parametric speed (the derivative $\mathrm{d}s/\mathrm{d}\xi$ of arc length with respect to the curve parameter ξ) and the curvature and torsion of $\mathbf{r}(\xi)$ being defined by

$$\sigma \,=\, |\mathbf{r}'|\,, \qquad \kappa \,=\, \frac{|\mathbf{r}' \times \mathbf{r}''|}{|\mathbf{r}'|^3}\,, \qquad \tau \,=\, \frac{(\mathbf{r}' \times \mathbf{r}'') \cdot \mathbf{r}'''}{|\mathbf{r}' \times \mathbf{r}''|^2}\,. \tag{3}$$

The relations (2) may be more succinctly expressed in the form

$$\frac{\mathrm{d}\mathbf{t}}{\mathrm{d}s} \,=\, \mathbf{d} \times \mathbf{t}\,, \qquad \frac{\mathrm{d}\mathbf{p}}{\mathrm{d}s} \,=\, \mathbf{d} \times \mathbf{p}\,, \qquad \frac{\mathrm{d}\mathbf{b}}{\mathrm{d}s} \,=\, \mathbf{d} \times \mathbf{b}\,, \tag{4}$$

where the *Darboux vector*

$$\mathbf{d} \;=\; \kappa\,\mathbf{b} \;+\; \tau\,\mathbf{t}\,, \tag{5}$$

named after Jean Gaston Darboux (1842–1917), defines the *angular velocity* of the Frenet–Serret frame, on traversing the curve at unit speed ($\mathrm{d}s/\mathrm{d}t \equiv 1$).

Despite its fundamental nature, the Frenet–Serret frame (1) is not without shortcomings. In general, on a polynomial or rational curve $\mathbf{r}(\xi)$, none of the frame vectors $(\mathbf{t}, \mathbf{p}, \mathbf{b})$ depend rationally on the curve parameter, making it difficult to ensure rational surfaces as the outcome of sweep operations. At an *inflection* of the curve (i.e., a point where $\kappa = 0$) the normal–plane vectors $\mathbf{p}$ and $\mathbf{b}$ are indeterminate, and generally suffer a sudden inversion on passing through such points. Finally, the insistence of $\mathbf{p}$ on pointing to the center of curvature is, in certain contexts, a nuisance rather than an advantage.

It is possible to identify certain special curves with rational Frenet–Serret frames [51], which correspond to the *double PH* (DPH) *curves* [16, 17, 47] — a subset of the spatial PH curves described in Section 3 below, characterized by the property that $|\,\mathbf{r}'(\xi)\,|$ and $|\,\mathbf{r}'(\xi) \times \mathbf{r}''(\xi)\,|$ are *both* polynomials in ξ. Every DPH curve of degree ≤ 5 is a *helical* curve, whose tangent maintains a constant inclination ψ with respect to a fixed direction (the *axis* of the helix) — equivalently, the ratio of curvature to torsion has the constant value $\tan\psi$. However, these curves are of relatively limited scope, and do not remedy the other shortcomings of the Frenet–Serret frame mentioned above.

In the Darboux vector (5), the term $\tau\,\mathbf{t}$ specifies a rotation rate for the normal–plane vectors $\mathbf{p}, \mathbf{b}$ about the tangent $\mathbf{t}$. This term is superfluous to an adapted frame comprising the tangent and two vectors that span the normal plane at each point, and by eliminating it one can find normal–plane vectors $\mathbf{u}, \mathbf{v}$ that do not rotate about $\mathbf{t}$. This fact was observed in the paper *There is more than one way to frame a curve* [3] by Bishop, who couched the problem in terms of *parallel transport* of the vectors $\mathbf{u}, \mathbf{v}$ along the curve — from any initial orientation, the variation of $\mathbf{u}, \mathbf{v}$ should be only such as to suffice to keep them in the normal plane, i.e., their derivatives must always be parallel to $\mathbf{t}$. Since the construction of such "relatively parallel" normal–plane vector fields is an initial–value problem, any curve admits a one–parameter family of rotation–minimizing adapted frames, also called [45, 49, 54] *Bishop frames*. The Frenet and rotation–minimizing frames are compared in Figure 1.

The rotation–minimizing or Bishop frame has a physical interpretation in the theory of elasticity. When an initially straight and uniform elastic rod

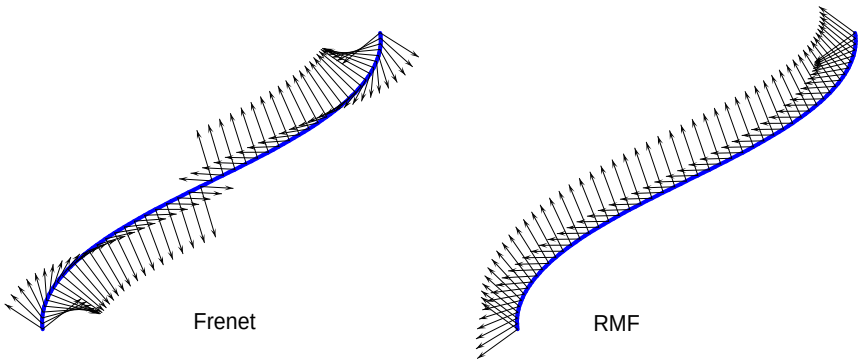

Figure 1: Comparison of Frenet frame (left) and rotation–minimizing frame (right) on a space curve with an inflection point (for clarity, only the normal–plane vectors are shown). Note the sudden inversion of the principal normal and binormal vectors in the Frenet frame, on passing through the inflection.

is deformed into a general smooth shape, the stored strain energy consists of *bending* and *twist* components. The former depends only on the curvature, while the latter is determined by the variation of normal–plane vectors along the deformed shape, that were initially invariant along the undeformed rod.[2] Among all possible variations of the normal–plane vectors, that defined by a rotation–minimizing frame has least (zero) twist energy [23, 46]. The twist of framed space curves is also of interest in analyzing DNA structure [5].

An important application for the rotation–minimizing frames arises in the construction of the *swept surfaces* generated by the motion of a closed planar profile curve along a spatial sweep curve, such that the profile curve always lies in the sweep curve normal plane. In this context, Klok [40] compared the results obtained by using the Frenet–Serret and rotation–minimizing frames to define the orientation of the profile curve within the sweep curve normal plane. Typically, the latter choice results in surfaces of superior shape (and parameterization). In [40], the RMF normal–plane vectors are characterized as solutions to the differential equation

$$\mathbf{w}'(\xi) \;=\; -\,\frac{\mathbf{r}''(\xi)\cdot\mathbf{w}(\xi)}{|\mathbf{r}'(\xi)|^2}\;\mathbf{r}'(\xi)\,,$$

[2]The variation of twist along the rod can be freely specified, and should not be confused with the torsion, which is purely a function of the deformed shape.

where $\mathbf{w}(\xi) = \mathbf{u}(\xi)$ or $\mathbf{v}(\xi)$. As noted by Guggenheimer [31], this prescription is equivalent to specifying the RMF vectors $\mathbf{u}, \mathbf{v}$ relative to $\mathbf{p}, \mathbf{b}$ through a rotation of the form

$$\begin{bmatrix} \mathbf{u}(\xi) \\ \mathbf{v}(\xi) \end{bmatrix} = \begin{bmatrix} \cos\theta(\xi) & \sin\theta(\xi) \\ -\sin\theta(\xi) & \cos\theta(\xi) \end{bmatrix} \begin{bmatrix} \mathbf{p}(\xi) \\ \mathbf{b}(\xi) \end{bmatrix} . \tag{6}$$

where the rotation angle $\theta(\xi)$ is defined by

$$\theta(\xi) \;=\; \theta_0 \;-\; \int_0^{\xi} \tau(u)\, \sigma(u)\, \mathrm{d}u \,. \tag{7}$$

Note that an incorrect sign before the integral is given in [31]. Since $\mathrm{d}\theta/\mathrm{d}s = -\tau$, this prescription exactly cancels the component τ of the angular velocity in the direction of $\mathbf{t}$ that appears in the Darboux vector (5). The integration constant θ_0 reflects the freedom in choosing the orientation of the initial RMF vectors $\mathbf{u}(0), \mathbf{v}(0)$. A trivial corollary of (6) and (7) is that the Frenet–Serret frame is an RMF for any planar curve, satisfying $\tau(\xi) \equiv 0$.

Although equations (6) and (7) constitute a closed–form definition for the RMF, it has some shortcomings. For general polynomial and rational curves, the integral in (7) has no closed–form reduction, and must be evaluated by numerical quadrature. Also $\mathbf{u}(\xi)$ and $\mathbf{v}(\xi)$ as defined by (6) are indeterminate at the inflections of $\mathbf{r}(\xi)$ — in order to ensure continuity through inflection points, an appropriate limit argument must be invoked.

Ideally, an exact (rational) representation is desirable for the RMF vectors $(\mathbf{t}(\xi), \mathbf{u}(\xi), \mathbf{v}(\xi))$. To achieve this, one must focus on *Pythagorean–hodograph* (PH) *curves*, since only the PH curves possess rational unit tangent vectors. Moreover, as described below, the PH curves admit a rational adapted frame, the *Euler–Rodrigues frame* (ERF), the circumvents the defects of the Frenet–Serret frame as a reference for computing rational RMFs [7].

3 Spatial Pythagorean–hodograph curves

We focus here on *polynomial* PH curves. Rational PH curves employ entirely different methods for their construction [30, 41] and, in general, do not admit rational arc lengths. A discussion of the use of the Möbius transformation in $\mathbb{R}^3$ to generate rational curves with rational RMFs may be found in [1].

The distinctive feature of a polynomial PH curve $\mathbf{r}(\xi) = (x(\xi), y(\xi), z(\xi))$ is that the components of its derivative $\mathbf{r}'(\xi) = (x'(\xi), y'(\xi), z'(\xi))$ satisfy

$$x'^2(\xi) + y'^2(\xi) + z'^2(\xi) \;=\; \sigma^2(\xi) \tag{8}$$

for some polynomial $\sigma(\xi)$. The *quaternion* and *Hopf map* forms [9] are two alternative (equivalent) models for the construction of spatial PH curves that are *rotation–invariant* [13]. The former generates a Pythagorean hodograph from a quaternion[3] polynomial

$$\mathcal{A}(\xi) \;=\; u(\xi) + v(\xi)\,\mathbf{i} + p(\xi)\,\mathbf{j} + q(\xi)\,\mathbf{k}\,, \tag{9}$$

and its conjugate $\mathcal{A}^*(\xi) = u(\xi) - v(\xi)\,\mathbf{i} - p(\xi)\,\mathbf{j} - q(\xi)\,\mathbf{k}$ through the product

$$\begin{aligned}\mathbf{r}'(\xi) \;=\; \mathcal{A}(\xi)\,\mathbf{i}\,\mathcal{A}^*(\xi) \;=\; &[\,u^2(\xi) + v^2(\xi) - p^2(\xi) - q^2(\xi)\,]\,\mathbf{i} \\ &+\, 2\,[\,u(\xi)q(\xi) + v(\xi)p(\xi)\,]\,\mathbf{j} \;+\; 2\,[\,v(\xi)q(\xi) - u(\xi)p(\xi)\,]\,\mathbf{k}\,.\end{aligned} \tag{10}$$

The latter generates a Pythagorean hodograph from complex polynomials

$$\boldsymbol{\alpha}(\xi) \;=\; u(\xi) + \mathrm{i}\,v(\xi)\,, \quad \boldsymbol{\beta}(\xi) \;=\; q(\xi) + \mathrm{i}\,p(\xi) \tag{11}$$

through the form

$$\mathbf{r}'(\xi) \;=\; (|\boldsymbol{\alpha}(\xi)|^2 - |\boldsymbol{\beta}(\xi)|^2, 2\,\mathrm{Re}(\boldsymbol{\alpha}(\xi)\overline{\boldsymbol{\beta}}(\xi)), 2\,\mathrm{Im}(\boldsymbol{\alpha}(\xi)\overline{\boldsymbol{\beta}}(\xi)))\,. \tag{12}$$

The equivalence of (10) and (12) can be verified by identifying the imaginary unit i with the quaternion element $\mathbf{i}$, and setting $\mathcal{A}(\xi) = \boldsymbol{\alpha}(\xi) + \mathbf{k}\,\boldsymbol{\beta}(\xi)$. We shall always assume, in (9) or (11), that $\gcd(u, v, p, q) =$ constant — this is a necessary, but not sufficient, condition for $\mathbf{r}'(\xi) = (x'(\xi), y'(\xi), z'(\xi))$ to be a *primitive* hodograph, i.e., $\gcd(x'(\xi), y'(\xi), z'(\xi)) =$ constant.

The parametric speed $\sigma(\xi) = |\mathbf{r}'(\xi)|$ of the curve defined by integrating (10) or (12) is the polynomial

$$\sigma(\xi) \;=\; |\mathcal{A}(\xi)|^2 \;=\; |\boldsymbol{\alpha}(\xi)|^2 + |\boldsymbol{\beta}(\xi)|^2 \;=\; u^2(\xi) + v^2(\xi) + p^2(\xi) + q^2(\xi)\,, \tag{13}$$

and integrating it gives the polynomial arc length function

$$s(\xi) \;=\; \int_0^\xi \sigma(u)\,\mathrm{d}u\,.$$

[3]The scalar and vector parts of a quaternion $\mathcal{A}$ are denoted by $\mathrm{scal}(\mathcal{A})$ and $\mathrm{vect}(\mathcal{A})$ — see Chapter 5 of [11] for a review of the quaternion algebra suited to the present context.

We consider here only *regular* curves, satisfying $\sigma(\xi) \neq 0$ for all real ξ.

Any spatial PH curve admits a closed–form reduction of the integral (7) specifying the orientation of the RMF vectors relative to the principal normal and binormal, through a partial–fraction decomposition of the integrand [10]. However, it is necessary to compute the complex–conjugate roots of $\sigma(\xi)$ and the resulting expression incorporates transcendental terms. We focus here on those PH curves for which the RMF admits an exact rational representation.

4 Euler–Rodrigues frame angular velocity

The *Euler–Rodrigues frame* (ERF) is a rational adapted orthonormal frame, defined on any spatial PH curve [7] through the expressions

$$(\mathbf{e}_1(\xi), \mathbf{e}_2(\xi), \mathbf{e}_3(\xi)) \;=\; \frac{(\mathcal{A}(\xi)\,\mathbf{i}\,\mathcal{A}^*(\xi), \mathcal{A}(\xi)\,\mathbf{j}\,\mathcal{A}^*(\xi), \mathcal{A}(\xi)\,\mathbf{k}\,\mathcal{A}^*(\xi))}{|\mathcal{A}(\xi)|^2}\,. \qquad (14)$$

The frame vector $\mathbf{e}_1(\xi)$ is the curve tangent, while $\mathbf{e}_2(\xi)$ and $\mathbf{e}_3(\xi)$ span the normal plane. In terms of the components of the quaternion polynomial (9) or complex polynomials (11), the frame vectors (14) are

$$\begin{aligned}
\mathbf{e}_1 \;&=\; \frac{(u^2+v^2-p^2-q^2)\,\mathbf{i} \;+\; 2(uq+vp)\,\mathbf{j} \;+\; 2(vq-up)\,\mathbf{k}}{u^2+v^2+p^2+q^2}\,,\\
\mathbf{e}_2 \;&=\; \frac{2(vp-uq)\,\mathbf{i} \;+\; (u^2-v^2+p^2-q^2)\,\mathbf{j} \;+\; 2(uv+pq)\,\mathbf{k}}{u^2+v^2+p^2+q^2}\,,\\
\mathbf{e}_3 \;&=\; \frac{2(up+vq)\,\mathbf{i} \;+\; 2(pq-uv)\,\mathbf{j} \;+\; (u^2-v^2-p^2+q^2)\,\mathbf{k}}{u^2+v^2+p^2+q^2}\,. \qquad (15)
\end{aligned}$$

The ERF variation is specified by its angular velocity[4] $\boldsymbol{\omega}$ through the relations

$$\mathbf{e}_1' \;=\; \boldsymbol{\omega} \times \mathbf{e}_1\,, \qquad \mathbf{e}_2' \;=\; \boldsymbol{\omega} \times \mathbf{e}_2\,, \qquad \mathbf{e}_3' \;=\; \boldsymbol{\omega} \times \mathbf{e}_3\,, \qquad (16)$$

and when $\boldsymbol{\omega}$ is expressed in terms of the ERF frame vectors as

$$\boldsymbol{\omega} \;=\; \omega_1\mathbf{e}_1 + \omega_2\mathbf{e}_2 + \omega_3\mathbf{e}_3\,, \qquad (17)$$

[4]Angular velocity is usually defined through time derivatives, or arc length derivatives (assuming a unit speed traversal). For brevity, we henceforth use derivatives with respect to the general parameter ξ. This does not materially alter any of the subsequent results.

its components are given by

$$\begin{aligned}
\omega_1 \;&=\; \mathbf{e}_3 \cdot \mathbf{e}_2' \;=\; -\,\mathbf{e}_2 \cdot \mathbf{e}_3' \;=\; \frac{2(uv' - u'v - pq' + p'q)}{u^2+v^2+p^2+q^2}\,, \\
\omega_2 \;&=\; \mathbf{e}_1 \cdot \mathbf{e}_3' \;=\; -\,\mathbf{e}_3 \cdot \mathbf{e}_1' \;=\; \frac{2(up' - u'p + vq' - v'q)}{u^2+v^2+p^2+q^2}\,, \\
\omega_3 \;&=\; \mathbf{e}_2 \cdot \mathbf{e}_1' \;=\; -\,\mathbf{e}_1 \cdot \mathbf{e}_2' \;=\; \frac{2(uq' - u'q - vp' + v'p)}{u^2+v^2+p^2+q^2}\,.
\end{aligned} \tag{18}$$

From (15) and (17)–(18), one can verify that

$$\begin{aligned}
\sigma\,\boldsymbol{\omega} \;&=\; 2\,(uv' - u'v + pq' - p'q)\,\mathbf{i} \\
&+\; 2\,(up' - u'p - vq' + v'q)\,\mathbf{j} \\
&+\; 2\,(uq' - u'q + vp' - v'p)\,\mathbf{k} \;=\; 2\,\mathrm{vect}(\mathcal{A}'\mathcal{A}^*)\,.
\end{aligned}$$

Consequently, since $\sigma' = 2(uu' + vv' + pp' + qq') = 2\,\mathrm{scal}(\mathcal{A}'\mathcal{A}^*)$, we note that

$$\sigma'^2 + \sigma^2 |\boldsymbol{\omega}|^2 \;=\; 4\,|\mathcal{A}|^2 |\mathcal{A}'|^2\,.$$

The ω_1 component of the ERF angular velocity specifies the rotation rate of the normal–plane vectors $\mathbf{e}_2, \mathbf{e}_3$ about the curve tangent $\mathbf{e}_1 = \mathbf{t}$ — i.e., the deviation of the ERF from an RMF. The existence of low–degree PH curves for which the ERF is an RMF (i.e., $\omega_1 \equiv 0$) was first discussed in [7]. It was shown that any cubic or quintic with this property is degenerate (i.e., planar), but that non–degenerate degree 7 PH curves with rotation–minimizing ERFs exist, and an algebraic characterization for these curves was developed.

Even if the ERF is not rotation–minimizing, a spatial PH curve may have a rational RMF when a rational normal–plane rotation that maps $\mathbf{e}_2(\xi), \mathbf{e}_3(\xi)$ onto RMF vectors $\mathbf{u}(\xi), \mathbf{v}(\xi)$ exists. Such a rotation must be of the form

$$\begin{bmatrix} \mathbf{u}(\xi) \\ \mathbf{v}(\xi) \end{bmatrix} \;=\; \frac{1}{a^2(\xi) + b^2(\xi)} \begin{bmatrix} a^2(\xi) - b^2(\xi) & -2\,a(\xi)b(\xi) \\ 2\,a(\xi)b(\xi) & a^2(\xi) - b^2(\xi) \end{bmatrix} \begin{bmatrix} \mathbf{e}_2(\xi) \\ \mathbf{e}_3(\xi) \end{bmatrix}, \tag{19}$$

for polynomials $a(\xi)$ and $b(\xi)$, corresponding to the rotation angle

$$\theta(\xi) \;=\; -\,2 \arctan \frac{b(\xi)}{a(\xi)}\,. \tag{20}$$

Differentiating (20), we see that the normal–plane rotation (19) has angular velocity $\theta' = 2(a'b - ab')/(a^2 + b^2)$ in the direction of $\mathbf{e}_1 = \mathbf{t}$. If $\mathbf{u}$ and $\mathbf{v}$ are

to be rotation–minimizing, this must exactly cancel ω_1, i.e., the components of (9) must be such as to ensure satisfaction of the condition

$$\frac{uv' - u'v - pq' + p'q}{u^2 + v^2 + p^2 + q^2} = \frac{ab' - a'b}{a^2 + b^2} \tag{21}$$

for some polynomials $a(\xi)$, $b(\xi)$ with $\gcd(a(\xi), b(\xi)) = \text{constant}$. This result was first derived in [32] and used to prove that non–planar PH cubics cannot have rational RMFs. The function on the left in (21) can be more compactly expressed as $\text{scal}(\mathcal{A}\,\mathbf{i}\,\mathcal{A}'^*)/|\mathcal{A}|^2$. For the Hopf map representation, condition (21) is equivalent to requiring the existence of a complex polynomial $\mathbf{w}(\xi) = a(\xi) + \mathrm{i}\, b(\xi)$, with $\gcd(a(\xi), b(\xi)) = \text{constant}$, such that

$$\frac{\text{Im}(\overline{\boldsymbol{\alpha}}\boldsymbol{\alpha}' + \overline{\boldsymbol{\beta}}\boldsymbol{\beta}')}{|\boldsymbol{\alpha}|^2 + |\boldsymbol{\beta}|^2} = \frac{\text{Im}(\overline{\mathbf{w}}\mathbf{w}')}{|\mathbf{w}|^2}\,. \tag{22}$$

Equation (21) is the fundamental constraint identifying those PH curves that admit rational rotation–minimizing frames, henceforth called *RRMF curves*. Curves for which the ERF is itself rotation–minimizing are subsumed as the special case where $a(\xi)$, $b(\xi)$ are constants, so that $ab' - a'b \equiv 0$.

For a quaternion polynomial (9) of degree m, defining a PH curve of odd degree $n = 2m+1$, the generic solutions to (21) involve polynomials $a(\xi), b(\xi)$ of degree m. However, solutions may also arise [29] for which $\deg(a, b) < m$, through a cancellation of factors common to the numerator and denominator on the left in (21). Such curves define a subspace of the set of RRMF curves of given degree. To distinguish between these different possibilities, the curves satisfying (21) with $\deg(a, b) = m, \ldots, 0$ are known [29] as *Class* $1, \ldots, m+1$ *RRMF curves* of degree $2m + 1$. For example, the degree 7 curves that have rotation–minimizing ERFs identified in [7] are Class 4 RRMF curves.

5 Rational rotation–minimizing frames

We now enumerate the known characterizations for non–degenerate types of low–degree RRMF curves satisfying (21) with $\deg(u, v, p, q) \leq 3$. Algorithms to construct each type may be found in the cited references. These algorithms also furnish the polynomials $a(\xi)$, $b(\xi)$ occurring on the right in (21), which are required to compute the associated rational RMFs through (19).

5.1 Class 1 RRMF quintics

The simplest and most intensively studied RRMF curves are Class 1 quintics. A PH quintic is generated by substituting a quadratic quaternion polynomial

$$\mathcal{A}(\xi) \;=\; \mathcal{A}_0(1-\xi)^2 + \mathcal{A}_1 2(1-\xi)\xi + \mathcal{A}_2\xi^2 \tag{23}$$

into expression (10) and integrating. Alternatively, for the Hopf map form, we substitute in (12) the two complex quadratic polynomials

$$\begin{aligned} \boldsymbol{\alpha}(\xi) \;&=\; \boldsymbol{\alpha}_0\,(1-\xi)^2 + \boldsymbol{\alpha}_1\,2(1-\xi)\xi + \boldsymbol{\alpha}_2\,\xi^2\,, \\ \boldsymbol{\beta}(\xi) \;&=\; \boldsymbol{\beta}_0\,(1-\xi)^2 + \boldsymbol{\beta}_1\,2(1-\xi)\xi + \boldsymbol{\beta}_2\,\xi^2\,. \end{aligned} \tag{24}$$

The first characterization of the Class 1 RRMF quintics involved constraints of degree 4 and 6 on the coefficients of the two complex polynomials (24) used in the Hopf map form [18]. However, these constraints were not symmetric with respect to reversing the order of the coefficient indices $0, 1, 2$ (a desirable property, corresponding merely to the re–parameterization $\xi \rightarrow 1-\xi$).

A much simpler characterization, phrased in terms of both the quaternion and Hopf map forms, was subsequently developed [12]. This characterization involves only quadratic coefficient constraints, and has the desired coefficient index symmetry. It may be summarized as follows.

Proposition 5.1. *A spatial PH quintic defined by the quaternion form* (10) *has a rational RMF if and only if the coefficients of the quaternion polynomial* (23) *satisfy*

$$\mathrm{vect}(\mathcal{A}_2\,\mathbf{i}\,\mathcal{A}_0^*) \;=\; \mathcal{A}_1\,\mathbf{i}\,\mathcal{A}_1^*\,. \tag{25}$$

For the Hopf map form (12)*, the corresponding conditions on the coefficients of the complex polynomials* (24) *are*

$$\mathrm{Re}(\boldsymbol{\alpha}_0\overline{\boldsymbol{\alpha}}_2 - \boldsymbol{\beta}_0\overline{\boldsymbol{\beta}}_2) \;=\; |\boldsymbol{\alpha}_1|^2 - |\boldsymbol{\beta}_1|^2\,, \quad \boldsymbol{\alpha}_0\overline{\boldsymbol{\beta}}_2 + \boldsymbol{\alpha}_2\overline{\boldsymbol{\beta}}_0 \;=\; 2\,\boldsymbol{\alpha}_1\overline{\boldsymbol{\beta}}_1\,. \tag{26}$$

A key step in simplifying the derivation is the reduction to *canonical form*, in which $\mathcal{A}_0 = 1$ for the quaternion form, and $(\boldsymbol{\alpha}_0, \boldsymbol{\beta}_0) = (1, 0)$ for the Hopf map form. For a regular curve with $\mathbf{r}'(0) \neq \mathbf{0}$, this can always be achieved by a scaling/rotation transformation in $\mathbb{R}^3$. Complete details on the derivation of Proposition 5.1 can be found in [12]. Note that $\mathrm{vect}(\mathcal{A}_0\,\mathbf{i}\,\mathcal{A}_2^*) = \mathrm{vect}(\mathcal{A}_2\,\mathbf{i}\,\mathcal{A}_0^*)$, so (25) has the desired symmetry; the symmetry of (26) is obvious.

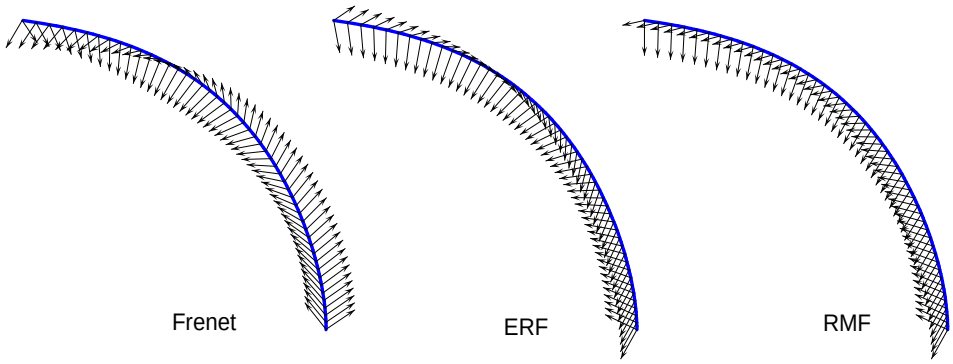

Figure 2: Comparison of adapted frames defined on a Class 1 RRMF quintic — from left to right: the Frenet frame, Euler–Rodrigues frame, and rational rotation–minimizing frame. Only the normal–plane vectors are shown here.

Figure 2 compares the Frenet frame, Euler–Rodrigues frame, and rational rotation–minimizing frame on a class 1 RRMF quintic, satisfying (25) with $\mathcal{A}_0 = 1 + 2\,\mathbf{i} + \mathbf{j} - 2\,\mathbf{k}$, $\mathcal{A}_1 = (1 + \mathbf{i} + \mathbf{j} - 3\,\mathbf{k})/\sqrt{2}$, $\mathcal{A}_2 = 2 - \mathbf{i} + 2\,\mathbf{j} - \mathbf{k}$. The corresponding Bernstein coefficients of the polynomials $a(\xi)$ and $b(\xi)$ in (21) are $(a_0, a_1, a_2) = (1, 1/\sqrt{2}, 3/5)$ and $(b_0, b_1, b_2) = (0, 0, -4/5)$. The angular velocities of the Frenet frame and rational RMF are illustrated in Figure 3.

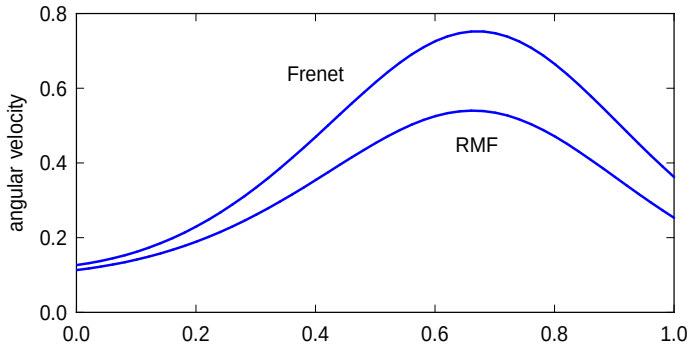

Figure 3: Comparison of angular velocities for the Frenet frame and rational rotation–minimizing frame on the Class 1 RRMF quintic shown in Figure 2.

Since (25) is a vector constraint, it determines any one of $\mathcal{A}_0, \mathcal{A}_1, \mathcal{A}_2$ in terms of the other two and a free parameter. Regarding $\mathcal{A}_0, \mathcal{A}_1, \mathcal{A}_2$ as points in $\mathbb{R}^4$, the following geometrical interpretation of (25) was derived in [22].

Proposition 5.2. *For given $\mathcal{A}_0$, $\mathcal{A}_2$ let $\mathbf{w} = w_x\mathbf{i}+w_y\mathbf{j}+w_z\mathbf{k} = \mathrm{vect}(\mathcal{A}_2\,\mathbf{i}\,\mathcal{A}_0^*)$, and in terms of $(\lambda,\mu,\nu) = (w_x,w_y,w_z)/|\mathbf{w}|$ define the unit quaternions*

$$\mathcal{E}_1 \;=\; 1 - \frac{\nu}{1+\lambda}\,\mathbf{j} + \frac{\mu}{1+\lambda}\,\mathbf{k}\,, \qquad \mathcal{E}_2 \;=\; \mathbf{i} + \frac{\mu}{1+\lambda}\,\mathbf{j} + \frac{\nu}{1+\lambda}\,\mathbf{k}\,,$$

which may be regarded as orthonormal vectors in $\mathbb{R}^4$. Then condition (25) is satisfied if and only if $\mathcal{A}_1$ lies on the circle in $\mathbb{R}^4$ specified by

$$\mathcal{A}_1(\phi) \;=\; \sqrt{\tfrac{1}{2}(1+\lambda)|\mathbf{w}|}\;(\cos\phi\;\mathcal{E}_2 - \sin\phi\;\mathcal{E}_1)\,.$$

The preceding results characterize Class 1 RRMF quintics by constraints on the coefficients of the pre–image polynomial (23). Apart from a constant factor, a polynomial can be specified by its coefficients or its roots. Because of the non–commutative nature of the quaternion product, the problems of defining and computing the roots of polynomials with quaternion coefficients are more subtle than in the real or complex case. An algorithm for the case of quadratic quaternion polynomials was described in [14], and used to derive the following characterizations for Class 1 RRMF quintics.

Lemma 5.1. *If a quadratic quaternion polynomial generating a Class 1 RRMF quintic has a double root the curve is degenerate, i.e., planar or linear.*

Proposition 5.3. *The quadratic quaternion polynomials that generate Class 1 RRMF quintics have roots $\mathcal{Q} = \lambda\,(q,\mathbf{q})$ where $\lambda > 0$ while q and $\mathbf{q}$ depend on a real value b, a unit vector $\mathbf{b} = (b_x,b_y,b_z)$, and a parameter $\tau \in [\,-1,+1\,]$ through the expressions*

$$q \;=\; \frac{1}{2}\left(-\,b \pm |\tau|\,\sqrt{\frac{1+b_x^2}{1-\tau^2}}\right)\,,$$

$$\begin{aligned}\mathbf{q} \;&=\; \frac{-\,b_x(b_x^2+\tau^2)\,\mathbf{i} - (1+b_x^2)\,[\,(b_y-b_z\tau)\,\mathbf{j} + (b_z+b_y\tau)\,\mathbf{k}\,]}{2\,(1+b_x^2\tau^2)} \\ &\mp\; \mathrm{sign}(\tau)\sqrt{\frac{1+b_x^2}{1-\tau^2}}\;\frac{(b_x^2+\tau^2)\,\mathbf{i} + b_x(1-\tau^2)\,[\,(b_y-b_z\tau)\,\mathbf{j} + (b_z+b_y\tau)\,\mathbf{k}\,]}{2\,(1+b_x^2\tau^2)}\,.\end{aligned}$$

It is not easy to extend these results to higher–order curves. Determining the roots of a quadratic quaternion polynomial entails the solution of a (real) cubic equation by Cardano's method. Higher–order quaternion polynomials have, in general, no closed–form solutions for their roots.

5.2 Class 2 RRMF quintics

The existence of non–planar Class 2 RRMF quintics was first established in [29]. As observed in [7], there are no non–planar Class 3 RRMF quintics (i.e., quintics with rotation–minimizing ERFs), so the classification of all possible RRMF quintics is complete. In characterizing the Class 1 RRMF quintics, a canonical form through a scaling/rotation transformation that maps $\mathbf{r}'(0)$ to the unit vector $\mathbf{i}$ was adopted. However, a different transformation is better suited to the analysis of Class 2 curves. Specifically, a *normal form* reduction is invoked, through which the components of (9) become

$$u(t) = t^2 + u_1 t + u_0, \;\; v(t) = v_1 t + v_0, \;\; p(t) = p_1 t + p_0, \;\; q(t) = q_1 t + q_0. \quad (27)$$

This reduction is always possible when $\mathcal{A}(t)$ is of true degree 2, and facilitates [29] the following characterization.

Proposition 5.4. *In normal form, the Class 2 RRMF quintics satisfying* (21) *with* $\deg(u, v, p, q) = 2$ *and* $\deg(a, b) = 1$ *are defined by* (27) *when* u_0, v_0, p_0, q_0 *are given in terms of free parameters* r, u_1, v_1, p_1, q_1 *with* $v_1 \neq 0$ *by*

$$\begin{aligned} u_0 &= -(u_1 + r)r \, - \, 4v_1^2(p_1^2 + q_1^2)/\Delta \,, \\ v_0 &= (u_1 + r)v_1 \,, \\ p_0 &= v_1 q_1 - p_1 r \, + \, 4v_1^2((u_1 + 2r)p_1 - 3v_1 q_1)/\Delta \,, \\ q_0 &= -(v_1 p_1 + q_1 r) \, + \, 4v_1^2((u_1 + 2r)q_1 + 3v_1 p_1)/\Delta \,, \end{aligned}$$

where $\Delta = (u_1 + 2r)^2 + 9v_1^2 + p_1^2 + q_1^2$.

This formulation allows one to construct non–planar examples of the Class 2 RRMF quintics through purely algebraic methods, but is less favorable to the construction of such curves satisfying prescribed geometrical constraints than the characterization of Class 1 RRMF quintics in Proposition 5.1.

5.3 Degree 7 RRMF curves

In principle, the degree 7 RRMF curves can be categorized into four distinct classes — that satisfy (21) with $\deg(u, v, p, q) = 3$ and $\deg(a, b) = 3, 2, 1, 0$ — but thus far only one of them has been satisfactorily analyzed. Since RRMF quintics cannot match arbitrary first–order data in the rotation–minimizing

rigid–body motion Hermite interpolation problem [19], the extra degrees of freedom afforded by degree 7 RRMF curves are important, and the obvious next step is to attempt a complete characterization of them.

Remark 5.1. One might think that the method used to derive the conditions (25) and (26) that characterize the Class 1 RRMF quintics should be readily extensible to degree 7 Class 1 RRMF curves, generated by a cubic quaternion polynomial $\mathcal{A}(\xi)$ or complex polynomials $\boldsymbol{\alpha}(\xi)$, $\boldsymbol{\beta}(\xi)$ specified in Bernstein form. However, this problem has thus far defied concerted efforts to derive satisfyingly simple analogs to (25) and (26) for the degree 7 case.

The only degree 7 RRMF curves for which a complete characterization is known are the Class 4 curves, for which $a(\xi), b(\xi) = \text{constant}$. These curves were first described in [7]. A more compact characterizaton is obtained [24] by noting that, for such curves, the numerator on the left in (25) must vanish. This can be stated, in terms of the quaternion representation, as follows — see [24] for the equivalent constraints in the Hopf map representation.

Proposition 5.5. *The degree 7 RRMF curves of Class 4 are characterized by satisfaction of the five constraints*

$$\begin{aligned} \operatorname{scal}(\mathcal{A}_0 \,\mathbf{i}\, \mathcal{A}_1^*) \;&=\; \operatorname{scal}(\mathcal{A}_0 \,\mathbf{i}\, \mathcal{A}_2^*) \;=\; 0\,, \\ 3\operatorname{scal}(\mathcal{A}_1 \,\mathbf{i}\, \mathcal{A}_2^*) \;&+\; \operatorname{scal}(\mathcal{A}_0 \,\mathbf{i}\, \mathcal{A}_3^*) \;=\; 0\,, \\ \operatorname{scal}(\mathcal{A}_1 \,\mathbf{i}\, \mathcal{A}_3^*) \;&=\; \operatorname{scal}(\mathcal{A}_2 \,\mathbf{i}\, \mathcal{A}_3^*) \;=\; 0\,, \end{aligned} \tag{28}$$

on the Bernstein coefficients of the cubic quaternion polynomial $\mathcal{A}(\xi)$ in (10).

5.4 The divisibility condition

A characterization for Class 1 RRMF curves of any degree, phrased in terms of a polynomial divisibility condition, was identified in [27]. From (9) and its derivative, one can form the polynomials

$$\rho \;=\; (up' - u'p + vq' - v'q)^2 \;+\; (uq' - u'q - vp' + v'p)^2\,, \tag{29}$$

$$\eta \;=\; (uu' + vv' + pp' + qq')^2 \;+\; (uv' - u'v - pq' + p'q)^2\,, \tag{30}$$

which satisfy

$$\rho + \eta \;=\; (u^2 + v^2 + p^2 + q^2)(u'^2 + v'^2 + p'^2 + q'^2) \;=\; |\mathcal{A}|^2 |\mathcal{A}'|^2\,. \tag{31}$$

The polynomial $\rho(\xi)$ plays a key role in the theory of DPH curves [16, 17] — since any PH curve satisfies

$$| \mathbf{r}'(\xi) \times \mathbf{r}''(\xi) |^2 \;=\; 4\,\sigma^2(\xi)\,\rho(\xi)\,,$$

the condition for a DPH curve is simply that $\rho(\xi)$ must be a perfect square. The following result arises [27] in the context of RRMF curves.

Proposition 5.6. *A spatial PH curve generated from* (10) *by a quaternion polynomial* $\mathcal{A}(\xi)$ *of any degree* m *is a Class 1 RRMF curve if and only if the polynomials* (29) *and* (30) *are divisible by the parametric speed* $\sigma = |\mathcal{A}|^2 = u^2 + v^2 + p^2 + q^2$.

The equivalence of Propositions 5.1 and 5.6 was shown, for RRMF quintics, in [28]. Because of (31), it is only necessary to check the divisibility of σ by either ρ or η. Notwithstanding its generality, the value of Proposition 5.6 in actually *constructing* higher–order RRMF curves is unclear.

5.5 Geodesics on ringed pre–image surface

The PH forms (10) and (12) both specify mappings from $\mathbb{R}^4$ to $\mathbb{R}^3$, for which the pre–image of any *point* in $\mathbb{R}^3$ is a *circle* in $\mathbb{R}^4$ with center at the origin. Consequently, the entire pre–image of any Pythagorean hodograph $\mathbf{r}'(\xi)$ is a *ringed surface* of the form

$$\mathcal{S}(\xi, \phi) \;=\; \mathcal{A}(\xi)\,\exp(\phi\,\mathbf{i})\,, \tag{32}$$

with $\exp(\phi\,\mathbf{i}) = (\cos\phi, \sin\phi\,\mathbf{i})$. The geometry of this surface was investigated in [22]. Any curve $\mathcal{C}(\xi) = \mathcal{S}(\xi, \phi(\xi))$ on the surface (32), specified by defining ϕ as a function of ξ, defines the same Pythagorean hodograph $\mathbf{r}'(\xi)$. However, it was shown in [22] that certain curves have a special significance for RMFs.

Proposition 5.7. *A curve* $\mathcal{C}(\xi) = \mathcal{S}(\xi, \phi(\xi))$ *on the ringed pre–image surface* (32) *in* $\mathbb{R}^4$ *that generates a rotation–minimizing frame on a spatial PH curve* $\mathbf{r}(\xi)$ *corresponds to a geodesic on that surface.*

To generate a *rational* RMF, $\phi(\xi)$ must be such that $\sin 2\,\phi(\xi)$ and $\cos 2\,\phi(\xi)$ are rational expressions in ξ. However, the corresponding pre–image curves $\mathcal{C}(\xi) = \mathcal{S}(\xi, \phi(\xi))$ are not, in general, rational geodesics on the surface (32).

6 Other rotation–minimizing frames

As previously noted, the most commonly–studied RMF is the *adapted* frame, which is rotation–minimizing with respect to the tangent $\mathbf{t}$. The Frenet frame is itself rotation–minimizing with respect to the principal normal $\mathbf{p}$. A third possibility, a frame that is rotation–minimizing with respect to the binormal $\mathbf{b}$, was studied in [20]. In the terminology of aerodynamics, these three frames define *roll–free*, *pitch–free*, and *yaw–free* motions. In the latter case, we speak of a rotation–minimizing *osculating* frame, since the rotation minimization is associated with the frame vectors in the curve osculating plane.

It was shown in [20] that no DPH curves of degree less than 7 with rational osculating RMFs exist. The study of curves with such frames was extended in [42] to the rational case, based on the dual representation [30, 41], and it was shown that rational curves with rational osculating RMFs of degree ≥ 6 exist, and the minimum degree of polynomial curves with this property is 7. The use of osculating RMFs to define ruled surfaces, with tangent planes matching the osculating planes of a given space curve, and rulings having the least rotation consistent with this constraint, was also discussed in [20, 42].

Rotation–minimizing *directed* frames, comprising the polar vector $\mathbf{o}(\xi) = \mathbf{r}(\xi)/|\mathbf{r}(\xi)|$ and two vectors $\mathbf{p}(\xi), \mathbf{q}(\xi)$ that span the *image plane* orthogonal to it, having no instantaneous rotation about $\mathbf{o}(\xi)$, were first considered in [15] — motivated by the problem of orienting a camera along a curved path. The theory for adapted RMFs carries over to the context of directed RMFs if all derivatives of $\mathbf{r}(\xi)$ are replaced by derivatives of order one less. Equivalently, one can replace $\mathbf{r}(\xi)$ by its *anti–hodograph*, i.e., indefinite integral. This leads to the notion of the *polar differential geometry* of $\mathbf{r}(\xi)$, involving the directed Frenet frame, polar curvature, polar torsion, etc. Correspondingly, to obtain a rational directed RMF, one must use *Pythagorean* (P) *curves* — satisfying $x^2(\xi)+y^2(\xi)+z^2(\xi) = \rho^2(\xi)$ for some polynomial $\rho(\xi)$ — in lieu of PH curves.

7 Applications of RRMF curves

7.1 Design of rigid–body motions

The construction of a *rational rotation–minimizing motion*, that interpolates prescribed initial/final positions $\mathbf{p}_i$, $\mathbf{p}_f$ and orientations $(\mathbf{t}_i, \mathbf{u}_i, \mathbf{v}_i)$, $(\mathbf{t}_f, \mathbf{u}_f, \mathbf{v}_f)$ of a rigid body, is a key application of the RRMF curves. This problem has

been studied in [19] for the case of Class 1 RRMF quintics, which nominally have sufficient freedoms to satisfy the specified boundary conditions. It was shown in [19] that interpolation of the end frames is always possible, while interpolation of the displacement $\mathbf{p}_f - \mathbf{p}_i$ reduces to finding the positive real roots of a degree 6 polynomial. However, it is possible to construct examples in which this polynomial has no real roots, and the non–linear dependence of its coefficients on the input data precludes simple *a priori* conditions for the existence of solutions (although it can be verified in the asymptotic case of sufficiently–dense data, sampled from a smooth curve).

An alternative approach to the problem, utilizing the degree 7 PH curves with rotation–minimizing ERFs, has been described in [24]. In this case, the problem can be reduced to solving a system of four quadratic equations in four real variables. These equations incorporate two free parameters, representing the magnitudes of the end derivatives, that can be used to optimize shape properties of the interpolant. In general, iterative numerical methods must be used to solve these equations and/or optimize the free parameters, and no formal proof of the existence of solutions for *some* parameter values is known. However, empirical evidence suggests that this is the case, and solutions are obtained in instances where the RRMF quintics admit none (see Figure 4).

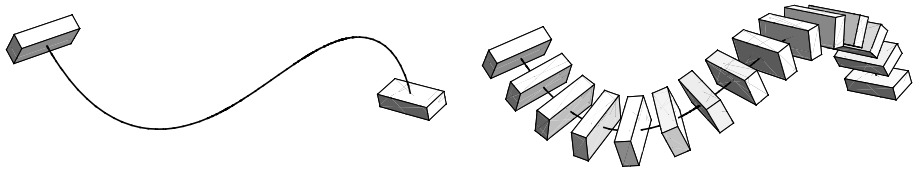

Figure 4: Example of a rational rotation–minimizing rigid–body motion with prescribed initial/final states, as specified by a Class 4 degree 7 RRMF curve.

Although the degree 7 interpolants are of higher degree than the RRMF quintics, their rational RMFs are actually of lower degree (6 versus 8), since they are coincident with the ERF and do not require a rational normal–plane rotation. Their main shortcoming, compared to the quintics, is their reliance on numerical solution methods, instead of a closed–form procedure.

7.2 5–axis tool orientation control

In 5–axis CNC machining of free–form surfaces with a ball–end cutter, it is desirable to employ a fixed angle ψ between the tool axis $\mathbf{a}$ and the surface normal $\mathbf{n}$ along the toolpath, so as to maintain a constant cutting speed. This leaves the azimuthal orientation of $\mathbf{a}$ about $\mathbf{n}$ indeterminate, and the idea of using a rotation–minimizing motion to fix it, so as to minimize actuation of the machine rotary axes, has been proposed in [26]. Relative to the *Darboux frame* $(\mathbf{t}, \mathbf{h}, \mathbf{n})$ consisting [44] of the path tangent $\mathbf{t}$, surface normal $\mathbf{n}$, and tangent normal $\mathbf{h} = \mathbf{n} \times \mathbf{t}$, the orientation of the tangent–plane component of $\mathbf{a}$ is specified as a constant minus the integral of the *geodesic curvature* [44] with respect to arc length along the toolpath. The inverse kinematics for such a motion, determining the machine axis inputs necessary to maintain the rotation–minimizing orientation of $\mathbf{a}$, have been studied in [25].

7.3 Swept surface constructions

The rotation–minimizing frames play an important role in the construction of *swept surfaces*, in which a surface is generated by the continuous spatial motion and/or deformation of a given "profile" curve [38, 40, 48]. The *canal surfaces* generated as the envelopes of one–parameter families of spheres with varying centers and radii are one example [6, 8] — in this case, using the RMF improves the quality of parameterization, but not the shape, of the surface. In the case of an asymmetric planar profile curve (e.g., an ellipse) that moves along a spatial sweep curve, so as to remain always in the sweep curve normal plane, using the adapted RMF to orient the profile curve within that plane can significantly improve the resulting swept surface shape — see Figure 5.

The adapted RMFs also have an intimate connection with certain intrinsic curves on a surface. The fact that the Darboux frame is rotation–minimizing with respect to the tangent along *lines of curvature* [44] on a smooth surface can be used to construct rational patches bounded by lines of curvature, by requiring the surface normal to coincide with any vector fixed relative to the RMF normal–plane vectors $\mathbf{u}, \mathbf{v}$. Complete details may be found in [2].

7.4 Rotation–minimizing camera motions

The rotation–minimizing directed frame was introduced in [15] as a means of reducing the apparent rotation of an object being imaged by an orientable

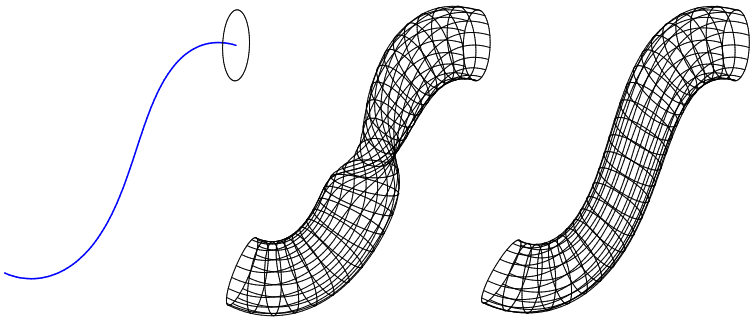

Figure 5: Swept surfaces generated by an ellipse that remains in the normal plane of a space curve (left) when the normal–plane orientation is specified through the Frenet frame (center) and the rotation–minimizing frame (right).

camera that traverses a curved path. Such frames have possible applications to endoscopic imaging or surgery, in which a miniature camera mounted on a flexible tube is inserted through a small incision, and directed along a curved path to image or sample tissue at a specific location in the body cavity. See [21, 33] for further development of the directed RMF algorithms.

8 Closure

Notwithstanding the considerable progress recently made in elucidating the characterization, properties, and construction algorithms for RRMF curves, the results surveyed herein indicate that significant gaps in the understanding and utilization of these curves still remain. This reflects the inherent difficulty of these remaining open problems, arising from their non–linear nature. We conclude by highlighting some of the key issues that remain unresolved.

- Proposition 5.1 gives an elegant and succinct characterization of Class 1 RRMF quintics, well–suited to use in construction algorithms. On the other hand, the identification of Class 2 RRMF quintics in Proposition 5.4 is rather opaque and complicated. A simpler description of these curves, better suited to geometrical construction algorithms, would be useful.

- Since the RRMF quintics have barely enough freedoms for geometrical interpolation problems, full development of the degree 7 RRMF curves

is desirable. Currently, only one of four possible classes of these curves has been satisfactorily categorized. An analog of Proposition 5.1, for the Class 1 degree 7 RRMF curves, remains to be developed.

- The divisibility condition for Class 1 RRMF curves in Proposition 5.6 is attractive, since it applies to curves of any degree. It would be useful to have methods that can apply this condition in a *constructive* manner.

- Currently available methods for designing rational rotation–minimizing motions by means of Hermite interpolation offer scope for improvement. The Class 1 RRMF quintics admit an essentially closed–form solution, but cannot accommodate arbitrary input data, while the Class 4 degree 7 RRMF curves provide free parameters but rely on iterative solution and/or optimization methods. A scheme offering a closed–form solution compatible with arbitrary initial/final states is desirable.

- Although the results obtained thus far are useful and non–trivial, they have been achieved on a case–by–case basis. An over–arching theory of RRMF curves, that could set the established results in proper context and help resolve the remaining open problems, is the ultimate goal.

References

[1] M. Barton, B. Jüttler, and W. Wang (2010), Construction of rational curves with rational rotation–minimizing frames via Möbius transformations, in *Mathematical Methods for Curves and Surfaces 2008*, Lecture Notes in Computer Science 5862, 15–25, Springer, Berlin.

[2] L. Biard, R. T. Farouki, and N. Szafran (2010), Construction of rational surface patches bounded by lines of curvature, *Comput. Aided Geom. Design* **27**, 359–371.

[3] R. L. Bishop (1975), There is more than one way to frame a curve, *Amer. Math. Monthly* **82**, 246–251.

[4] C. B. Boyer (2004), *History of Analytic Geometry*, Dover Publications, Mineola, New York (reprint).

[5] G. S. Chirikjian (2013), Framed curves and knotted DNA, *Biochem. Soc. Trans.* **41**, 635–638.

[6] H. C. Cho, H. I. Choi, and S. H. Kwon (2004), Clifford algebra, Lorentzian geometry, and rational parameterization of canal surfaces, *Comput. Aided Geom. Design* **21**, 327–339.

[7] H. I. Choi and C. Y. Han (2002), Euler–Rodrigues frames on spatial Pythagorean–hodograph curves, *Comput. Aided Geom. Design* **19**, 603–620.

[8] H. I. Choi, S. H. Kwon, and N. S. Wee (2004), Almost rotation–minimizing rational parameterization of canal surfaces, *Comput. Aided Geom. Design* **21**, 859–881.

[9] H. I. Choi, D. S. Lee, and H. P. Moon (2002), Clifford algebra, spin representation, and rational parameterization of curves and surfaces, *Adv. Comp. Math.* **17**, 5–48.

[10] R. T. Farouki (2002), Exact rotation–minimizing frames for spatial Pythagorean–hodograph curves, *Graph. Models* **64**, 382–395.

[11] R. T. Farouki (2008), *Pythagorean–Hodograph Curves: Algebra and Geometry Inseparable*, Springer, Berlin.

[12] R. T. Farouki (2010), Quaternion and Hopf map characterizations for the existence of rational rotation–minimizing frames on quintic space curves, *Adv. Comp. Math.* **33**, 331–348.

[13] R. T. Farouki, M. al–Kandari, and T. Sakkalis (2002), Structural invariance of spatial Pythagorean hodographs, *Comput. Aided Geom. Design* **19**, 395–407.

[14] R. T. Farouki, P. Dospra, and T. Sakkalis (2013), Scalar–vector algorithm for the roots of quadratic quaternion polynomials, and the characterization of quintic rational rotation–minimizing frame curves, *J. Symb. Comput.* **58**, 1–17.

[15] R. T. Farouki and C. Giannelli (2009), Spatial camera orientation control by rotation–minimizing directed frames, *Comput. Anim. Virt. Worlds* **20**, 457–472.

[16] R. T. Farouki, C. Giannelli, and A. Sestini (2009), Helical polynomial curves and double Pythagorean hodographs I. Quaternion and Hopf map representations, *J. Symb. Comput.* **44**, 161–179.

[17] R. T. Farouki, C. Giannelli, and A. Sestini (2009), Helical polynomial curves and double Pythagorean hodographs II. Enumeration of low–degree curves, *J. Symb. Comput.* **44**, 307–332.

[18] R. T. Farouki, C. Giannelli, C. Manni, and A. Sestini (2009), Quintic space curves with rational rotation–minimizing frames, *Comput. Aided Geom. Design* **26**, 580–592.

[19] R. T. Farouki, C. Giannelli, C. Manni, and A. Sestini (2012), Design of rational rotation–minimizing rigid body motions by Hermite interpolation, *Math. Comp.* **81**, 879–903.

[20] R. T. Farouki, C. Giannelli, M. L. Sampoli, and A. Sestini (2014), Rotation–minimizing osculating frames, *Comput. Aided Geom. Design* **31**, 27–42.

[21] R. T. Farouki, C. Giannelli, and A. Sestini (2013), An interpolation scheme for designing rational rotation–minimizing camera motions, *Adv. Comp. Math.* **38**, 63–82.

[22] R. T. Farouki and R. Gutierrez (2014), Geometry of the ringed surfaces in $\mathbb{R}^4$ that generate spatial Pythagorean hodographs, *J. Symb. Comput.* to appear.

[23] R. T. Farouki and C. Y. Han (2003), Rational approximation schemes for rotation–minimizing frames on Pythagorean–hodograph curves, *Comput. Aided Geom. Design* **20**, 435–454.

[24] R. T. Farouki, C. Y. Han, P. Dospra, and T. Sakkalis (2013), Rotation–minimizing Euler–Rodrigues rigid–body motion interpolants, *Comput. Aided Geom. Design* **30**, 653–671.

[25] R. T. Farouki, C. Y. Han, and S. Li (2014), Inverse kinematics for optimal tool orientation control in 5–axis CNC machining, *Comput. Aided Geom. Design* **31**, 13–26.

[26] R. T. Farouki and S. Li (2013), Optimal tool orientation control for 5–axis CNC milling with ball–end cutters, *Comput. Aided Geom. Design* **30**, 226–239.

[27] R. T. Farouki and T. Sakkalis (2010), Rational rotation–minimizing frames on polynomial space curves of arbitrary degree, *J. Symb. Comput.* **45**, 844–856.

[28] R. T. Farouki and T. Sakkalis (2011), Equivalence of distinct characterizations for rational rotation-minimizing frames on quintic space curves, *Comput. Aided Geom. Design* **28**, 436–445.

[29] R. T. Farouki and T. Sakkalis (2012), A complete classification of quintic space curves with rational rotation–minimizing frames, *J. Symb. Comput.* **47**, 214–226.

[30] R. T. Farouki and Z. Sir (2011), Rational Pythagorean–hodograph space curves, *Comput. Aided Geom. Design* **28**, 75-88.

[31] H. Guggenheimer (1989), Computing frames along a trajectory, *Comput. Aided Geom. Design* **6**, 77–78.

[32] C. Y. Han (2008), Nonexistence of rational rotation–minimizing frames on cubic curves, *Comput. Aided Geom. Design* **25**, 298–304.

[33] G. Jaklic, M. L. Sampoli, A. Sestini, and E. Zagar (2013), C^1 rational interpolation of spherical motions with rational rotation–minimizing directed frames, *Comput. Aided Geom. Design* **30**, 159–173.

[34] B. Jüttler (1998), Generating rational frames of space curves via Hermite interpolation with Pythagorean hodograph cubic splines, in *Geometric Modeling and Processing '98*, Bookplus Press, pp. 83–106.

[35] B. Jüttler (1998), Rotation minimizing spherical motions, in *Advances in Robot Kinematics: Analysis and Control* (J. Lenarcic and M. L. Husty, eds.), Springer, Dordrecht, pp. 413–422.

[36] B. Jüttler and C. Mäurer (1999), Cubic Pythagorean hodograph spline curves and applications to sweep surface modelling, *Comput. Aided Design* **31**, 73–83.

[37] B. Jüttler and C. Mäurer (1999), Rational approximation of rotation minimizing frames using Pythagorean–hodograph cubics, *J. Geom. Graphics* **3**, 141–159.

[38] B. Jüttler and M. G. Wagner (1999), Rational motion–based surface generation, *Comput. Aided Design* **31**, 203–213.

[39] M. Klein (1972), *Mathematical Thought from Ancient to Modern Times*, Volume 2, Oxford University Press, New York.

[40] F. Klok (1986), Two moving coordinate frames for sweeping along a 3D trajectory, *Comput. Aided Geom. Design* **3**, 217–229.

[41] J. Kozak, M. Krajnc, and V. Vitrih (2014), Dual representation of spatial rational Pythagorean–hodograph curves, *Comput. Aided Geom. Design* **31**, 43–56.

[42] J. Kozak, M. Krajnc, and V. Vitrih (2015), Parametric curves with Pythagorean binormal, *Adv. Comp. Math.* to appear.

[43] M. Krajnc and V. Vitrih (2012), Motion design with Euler–Rodrigues frames of quintic Pythagorean–hodograph curves, *Math. Comput. Simul.* **82**, 1696–1711.

[44] E. Kreyszig (1959), *Differential Geometry*, University of Toronto Press.

[45] H. M. Liu and D. H. Pei (2013), Singularities of a space curve according to the relatively parallel adapted frame and its visualization, *Math. Prob. Eng.* Article No. 512020.

[46] A. E. H. Love (1944), *A Treatise on the Mathematical Theory of Elasticity*, Dover (reprint), New York.

[47] J. Monterde (2009), A characterization of helical polynomial curves of any degree, *Adv. Comp. Math.* **30**, 61–78.

[48] H. Pottmann and M. G. Wagner (1998), Contributions to motion based surface design, *Int. J. Shape Model.* **4**, 183–196.

[49] J. M. Selig (2013), Characterization of Frenet–Serret and Bishop motions with applications to needle steering, *Robotica* **31**, 981–992.

[50] Z. Sir and B. Jüttler (2005), Spatial Pythagorean hodograph quintics and the approximation of pipe surfaces, in *Mathematics of Surfaces XI* (R. Martin, H. Bez, and M. Sabin, eds.) Springer, Berlin, pp. 364–380.

[51] M. Wagner and B. Ravani (1997), Curves with rational Frenet–Serret motion, *Comput. Aided Geom. Design* **15**, 79–101.

[52] W. Wang and B. Joe (1997), Robust computation of the rotation minimizing frame for sweep surface modelling, *Comput. Aided Design* **29**, 379–391.

[53] W. Wang, B. Jüttler, D. Zheng, and Y. Liu (2008), Computation of rotation minimizing frames, *ACM Trans. Graphics* **27**, Article 2, 1–18.

[54] S. Yilmaz and M. Turgut (2010), A new version of Bishop frame and an application to spherical images, *J. Math. Anal. Appl.* **371**, 764–776.

[55] Z. Zheng and G. Wang (2005), Constructing rotation–minimizing frame of space Bézier curve, *J. Comput. Aided Design & Comput. Graphics* **17**, 1785–1792.